Earth, Planets and Space

FULL PAPER Open Access

Mechanism of vertical displacement beneath shallow compression zone in coastal area

Duc-Huy Tran[1], Shih-Jung Wang[1,2*] and Jian-Yu Chen[1]

Abstract

Previous studies showed that there is a discrepancy between total subsidence (measured on the ground surface) and shallow compression (measured within several hundred meters beneath the ground surface) in Taiwan. This difference is referred to as deep displacement in this study. The variations of deep displacement are opposite to those of ground surface displacement and groundwater level within the depth of several hundred meters. The mechanism is unknown and requires further investigation. This study adopts two kinds of geodetic observation data and separates land subsidence into shallow compression and deep displacement to investigate the mechanism of deep displacement. A tectonically active coastal area in Taiwan is selected as the study area. The assessment results show that the associated variations are likely due to cyclic hydraulic loading and unloading. The variations of deep displacement are opposite to those of ground surface displacement. This study proposes that these variations are due to hydraulic expansion and contraction. The mechanism is demonstrated using a hydromechanical model. The results of a cross-correlation analysis show that hydraulic expansion and contraction occur at certain depths. The study results provide important information on the mechanism of deep displacement that can be used in tectonophysical and land subsidence investigations.

Keywords Land subsidence, Hydraulic expansion and contraction, Anthropogenic activity, Global Positioning System, Multi-layer compaction monitoring well

*Correspondence:
Shih-Jung Wang
sjwang@ncu.edu.tw
Full list of author information is available at the end of the article

Graphical Abstract

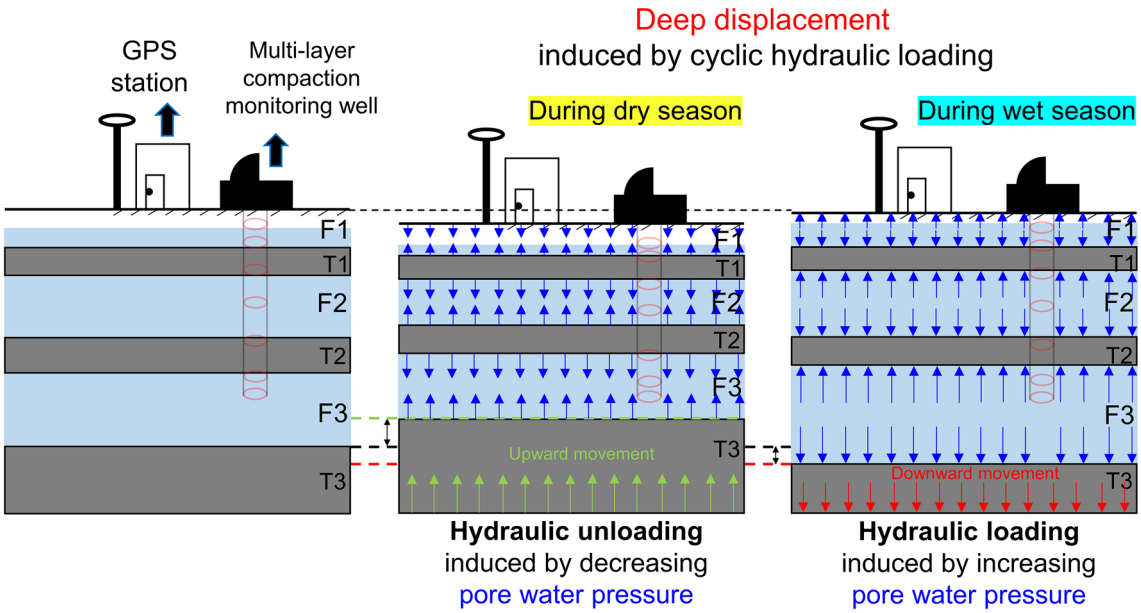

Introduction

Mechanisms induced by natural factors, such as natural compression, seasonal hydrological loading, tectonic activity, fault activity, and earthquakes, contribute to land subsidence. Fu et al. (2012), Chanard et al. (2014), and Hsu et al. (2020) reported that the seasonal hydrological loading of continental water storage and its loading effects are significant in southern Alaska, the Himalayas, and Taiwan, respectively. Hsu et al. (2021) found that the hydrological cycle in western Taiwan causes elastic loading and unloading effects, which may be the primary driving mechanism of the observed synchronized modulation of earthquakes. In the polar region or high-elevation areas in winter, frozen water and snow create mass loading on the ground surface, which can lead to land subsidence. The recovery of frozen soils in summer mainly depends on their physical properties (Martens 2016; Knappe et al. 2019). These mechanisms mainly induce land subsidence at shallow depths (on the scale of hundreds of meters). Carminati and Di Donato (1999) and Teatini et al. (2007) reported that there is a small natural subsidence in Italy (− 1.6 and − 1.2 mm/yr in Ravenna and Venice, respectively). Land subsidence can also be induced by tectonic activity, fault activity, creep, or continuous plate and fault movement (Wu 1978; Yu et al. 1997; Lacombe et al. 2001; Bos et al. 2003; Chiang et al. 2004; Shyu et al. 2005; Hu et al. 2006, 2007). Parsons (2006) reported that earthquakes result from elastic stress built up in part by tectonic motion. Earthquake events can induce a sudden change in displacement and tectonic activity and fault activity can induce a long-term movement of a plate or geological structure, inducing strata displacement in both the vertical and horizontal directions. These mechanisms mainly induce land subsidence at deep depths (on the scale of kilometers). However, the assessments in these studies did not always consider the influence of anthropogenic activity, especially in areas with dense populations, which resulted in large uncertainty in the assessment results.

In some delta regions, such as the Mekong Delta in Vietnam (Zoccarato et al. 2018), the Po Delta in Italy (Teatini et al. 2011), and the Mississippi Delta in the USA (Törnqvist et al. 2008; Jankowski et al. 2017), young sediments (e.g., Holocene sediments) commonly have a high compression rate because of a relatively loose sedimentary environment and high groundwater over-extraction. Liu et al. (2020) assumed that land subsidence has two components: (1) a contribution from bedrock systems or non-compressing strata caused by tectonic subsidence and (2) a contribution from the compression of compressible, non-bedrock aquifer systems caused by primary consolidation due to subsurface fluid withdrawal. Therefore, coastal areas with anthropogenic activity might have serious land subsidence due to shallow compression induced by construction loading and/or groundwater over-extraction (Poland 1984; Galloway et al. 1998;

Alley et al. 2002; Hou et al. 2005; Gambolati et al. 2006; Hu et al. 2006; Meckel et al. 2006; Hsu et al. 2007; Teatini et al. 2007; Hung et al. 2010; Galloway and Burbey 2011; Hsieh et al. 2011; Tung and Hu 2012; Erban et al. 2013; Wang et al. 2015a, 2015b; Hwang et al. 2016; Jones et al. 2016; Minderhoud et al. 2017; Tran et al. 2022). The depth at which anthropogenic activity-induced compression has influence is relatively shallow, but the contribution to land subsidence is relatively large compared to that of tectonic activity and plate displacement. Tectonophysical studies commonly use ground surface observation systems to assess tectonic activity and plate displacement (Yu et al. 1997; Bos et al. 2003; Hou et al. 2005; Shyu et al. 2005; Hu et al. 2006, 2007; Parsons 2006; Ching et al. 2007, 2011; Wang and Shen 2020). Therefore, the influence of anthropogenic activity can have a large effect on the investigation of mechanisms in tectonophysical studies.

Techniques such as leveling, the Global Positioning System (GPS), deep benchmarks, multi-layer compaction monitoring wells (MLCWs), and interferometric synthetic aperture radar (InSAR) are commonly used to monitor land subsidence. Leveling, GPS, and InSAR are used to monitor total subsidence on the ground surface and deep benchmarks and MLCWs are used to monitor compression within a certain depth range. Previous studies (Hung et al. 2010, 2018) showed that there is a discrepancy between total subsidence (measured by leveling and GPS) and shallow compression (measured by MLCWs) in Taiwan. This difference is caused by displacement beyond the major compression zone, which is referred to as deep displacement in this study. The mechanism of deep displacement is unknown due to a lack of direct observation data. Deep compression due to groundwater over-extraction has been proposed as a possible mechanism (e.g., Galloway et al. 1998; Erban et al. 2013; Hung et al. 2018). However, the variations of deep displacement are opposite to those of groundwater level variations at shallow depths (Tran and Wang 2020), which is inconsistent with deep compression due to groundwater over-extraction (Lu et al. 2020; Hsu et al. 2021). Further investigations are thus needed.

The coastal area of Pingtung Plain in Taiwan had the most substantial cumulative subsidence (3.56 m), which was mainly due to groundwater over-extraction, in the period 1972–2018 (Taiwan Water Resources Agency (WRA) 2018). Therefore, the WRA installed several subsidence and groundwater monitoring systems in this area. Previous studies reported that approximately three-quarters of land subsidence in Pingtung Plain is caused by groundwater over-extraction and that part of the remaining land subsidence is caused by tectonic activity (Kuo et al. 2001; Hou et al. 2005; Hu et al. 2006, 2007). However, these studies did not provide observation data to quantify land subsidence due to anthropogenic activity and natural factors and did not discuss the subsidence mechanisms at shallow and deep depths. Therefore, Pingtung Plain is a suitable location for validating the mechanism of vertical displacement due to natural (deep depth) and anthropogenic (shallow depth) factors. The present study uses multiple geodetic techniques to quantify and investigate land subsidence due to deep displacement in a tectonically active region. A coupled hydromechanical model is used to demonstrate the phenomenon of hydraulic expansion and contraction, defined in this study, for deep displacement.

Background

Study area

The study area is located in the coastal area of Pingtung Plain, Taiwan, for which there are sufficient data to investigate the mechanism of land subsidence (Fig. 1). A borehole log and a hydrogeological cross section between three wells, namely Dexing, Fangliao, and Jiadong wells, in the study area were constructed, as shown in Fig. 2A and B. According to the geological characteristics of the alluvial fan, the study area stretches from the proximal fan (Fangliao area) to the distal fan (Jiadong area). The energy available for the sediment process is low due to the apparent terrain elevation from the northeast to the southwest of Linbian River (Fig. 1B). The geological age has a marked change from 11,030 ± 60 to 29,200 ± 330 years ago; thus, the Holocene unconsolidated sediment is distributed within a depth of about 120 m (Fig. 2B). S-wave velocity and electrical resistivity data provide information on the lithology at Jiadong well, as shown in Fig. 2C. These data can be used as a reference for determining the depth of cemented sediment.

The tectonic processes in Pingtung Plain have two states (Fig. 1A), namely a dynamically extruded state in the east and southeast and a static state in the plain area, separating Pingtung Plain by the Chaochou active fault (Lacombe et al. 2001). There is a tectonic escape connected with a tectonic extrusion and a lateral extrusion that operates at the southern tip of the Taiwan collision belt, towards the submerged area in the Manila trench, and acts as a free boundary (Lacombe et al. 2001; Hou et al. 2005; Hu et al. 2006, 2007; Ching et al. 2007). Quaternary unconsolidated sediments form a basin and lie on the wedge-top depozone and associated piggyback basins (Chiang et al. 2004). They are caused by the weathering of the Taiwan orogeny and form the principal aquifer of Pingtung Plain.

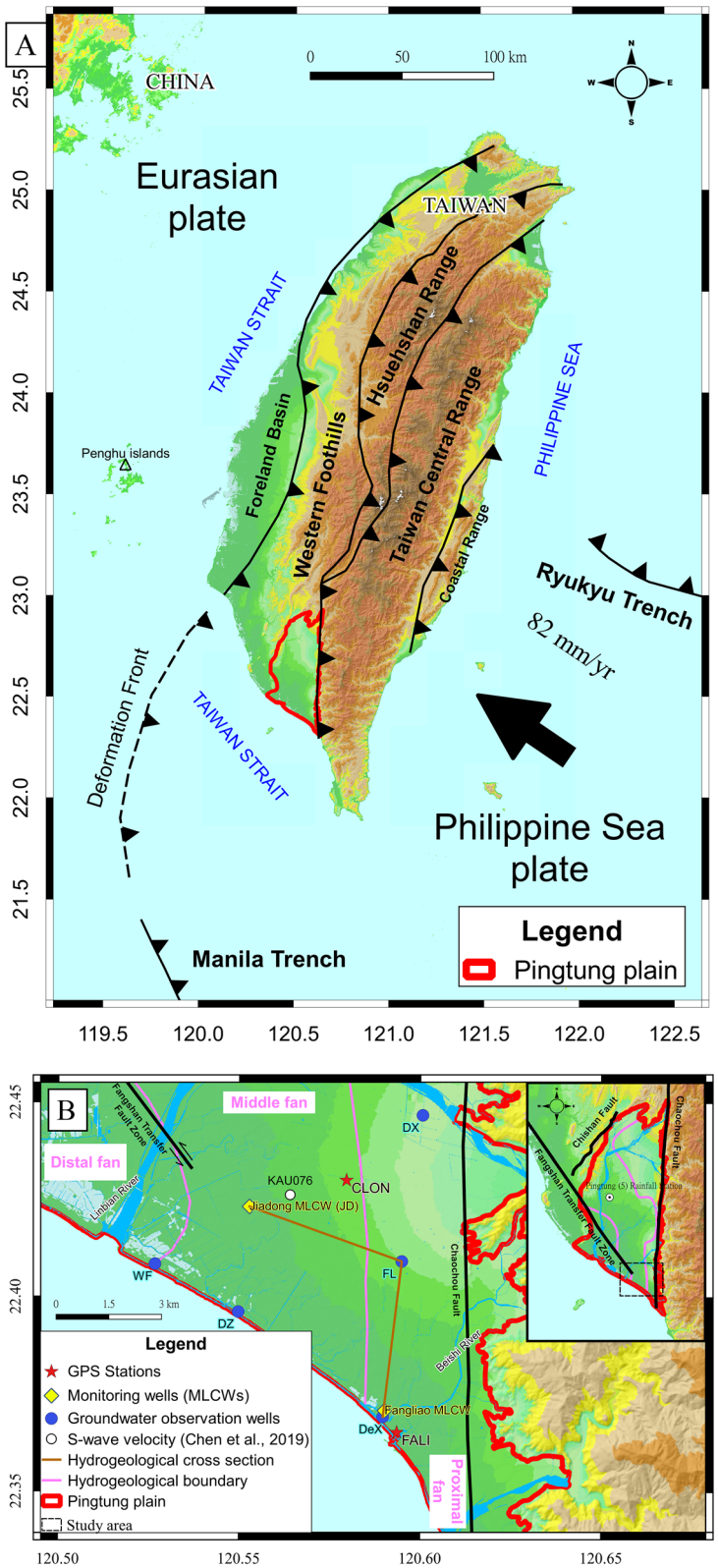

Fig. 1 General geological and monitoring settings. **A** Simplified tectonic framework in Taiwan, where tectonic information is from Yu et al. (1997) and Ching et al. (2007). **B** Distribution of land subsidence monitoring stations and groundwater level monitoring wells, where fault system is from Chiang (1971) and Ching et al. (2007).

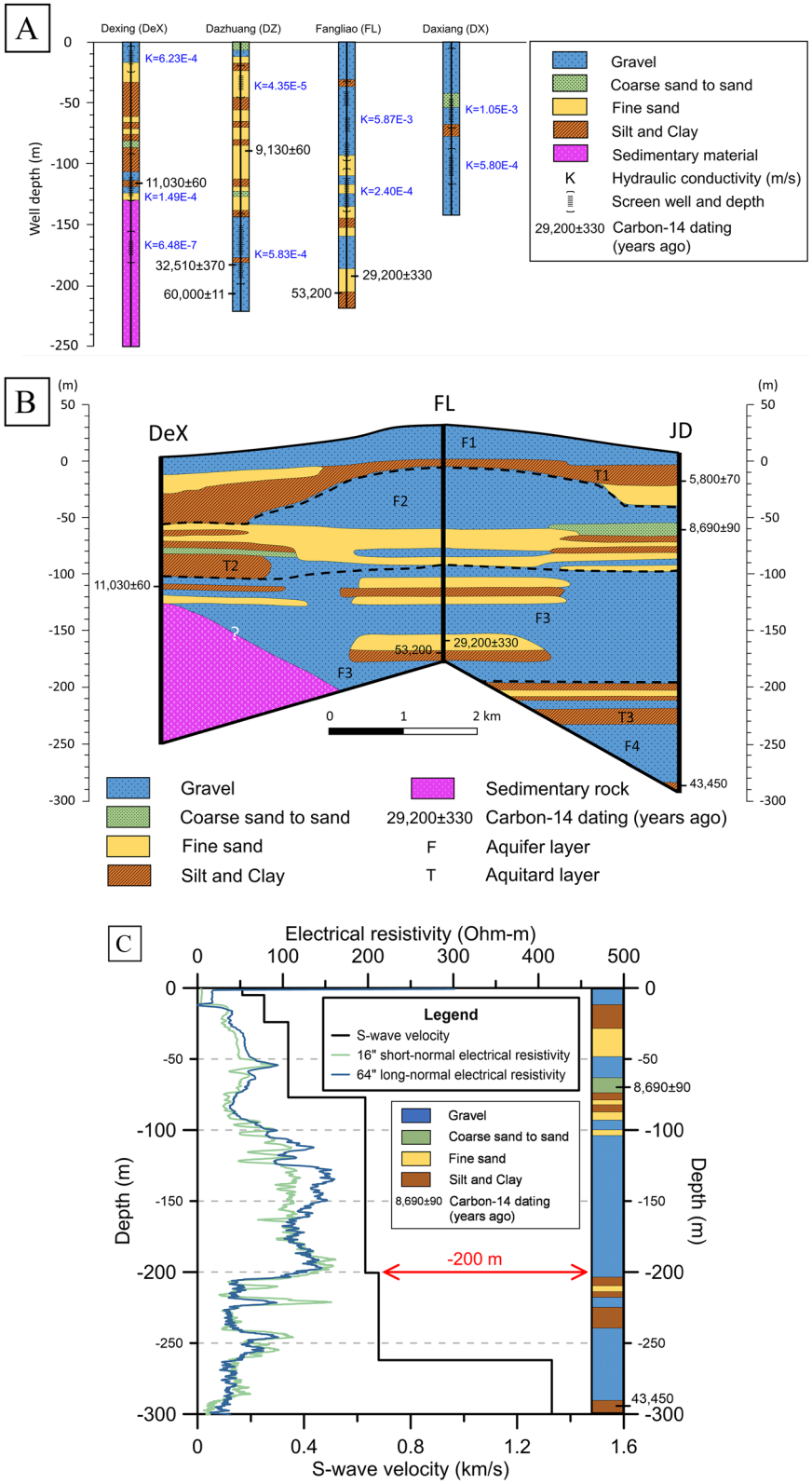

Fig. 2 Geological information. **A** Borehole log, **B** cross section of hydrogeology, and **C** S-wave velocity (Kuo et al. 2016; Chen et al. 2022) and electrical resistivity geophysical survey at Jiadong area with lithology from Geological Survey and Mining Management Agency (GSMMA). The trace of the hydrogeological profile and S-wave station are shown in Fig. 1

Monitoring systems and observation data

In Taiwan, four techniques are commonly used to observe land subsidence, namely leveling, GPS, MLCWs, and InSAR (Hung et al. 2010, 2021). MLCWs, developed in Taiwan, are used to measure the compression of the aquifer system in different layers (Hung et al. 2010). In this study, Jiadong and Fangliao MLCWs are adopted due to their long monitoring period and proximity to GPS stations, which measure deformation within 200 m from Earth's surface. GPS data are adopted due to their high sampling rate, which allows a displacement comparison at a given time point between two observation systems. Two GPS stations, named CLON and FALI, are selected in this study because they are the closest stations to the MLCWs. Furthermore, five monitoring wells, named Dazhuang (DZ), Wenfeng (WF), Daxiang (DX), Fangliao (FL), and Dexing (DeX), respectively, are used for groundwater level observation in the study area. The distribution of the observation systems is shown in Fig. 1B. Note that the observation stations are not completely collocated. It is assumed that for a given station, the closest station records similar behavior. In this study, the behaviors recorded at nearby stations are compared. The comparison of non-collocated data is a source of uncertainty in this study.

The observation data of hydrology and land subsidence in the study area from 2007 to 2016 are shown in Fig. 3. The variations of land subsidence, groundwater level, and rainfall quantity show similar patterns, which are induced by seasonal hydrological variations. The dry season is from November to April, during which there is a steady decline in the groundwater level due to small recharge and large discharge. Both anthropogenic (e.g., pumping for drinking water, irrigation, and aquaculture) and natural (e.g., evapotranspiration, submarine groundwater discharge, and baseflow) factors decrease the groundwater level, inducing the compression of porous media. The wet season is from May to October, during which precipitation is mainly from monsoon rains, plum rains, and typhoons, which largely increase groundwater recharge. Hence, groundwater level increases, leading to the dilation of porous media. Figure 4 shows the seasonal fluctuations of groundwater level in three aquifers (defined in Fig. 2B). The fluctuations are 0.82−32.78, 11.79−33.47, and 7.44−22.63 m for the first, second, and third aquifers, respectively. A good permeable aquifer lets water easily recharge into and discharge from the aquifer and induces a large variation of groundwater level.

Methodology

Deep displacement calculation

Based on the monitoring limit of MLCWs, vertical displacement was separated into a shallow component (within 200 m) and a deep component (beyond 200 m). In this study, the former is denoted as shallow compression and the latter is denoted as deep displacement. Note that this study does not attempt to define the threshold of deep displacement; it only collects observation data to investigate the mechanism of vertical displacement beneath the major compression zone. Different areas may have different thresholds for the vertical displacement, with different responses above and below the threshold.

To obtain the accurate results of deep displacement, both the GPS and MLCW data need to be assessed carefully. Satellite signals (e.g., GPS) are adversely influenced by the atmosphere and air pressure variations. It is difficult to avoid numerical errors when using real-time resampling. The measurement period of MLCWs is about 1 month, whereas that of continuous GPS is 1 day. Therefore, the weekly average from the mid-point solution of GPS data is calculated to reduce numerical errors. The measurement date of MLCW data is the reference point. GPS data collected within three days before and after the reference date of MLCW data are averaged (for a total of 7 GPS data points). The MLCW data obtained at the same time point are subtracted from the averaged results of GPS data to calculate their difference (i.e., the deep displacement). Deep displacement is calculated at each time point of MLCW data to obtain the time series of deep displacement.

Hydromechanical model

A coupled hydromechanical model is used to demonstrate the phenomenon of hydraulic expansion and contraction proposed in this study. The commercial software COMSOL Multiphysics and poroelastic theory are adopted for the simulation. The governing equation for fluid mass conservation can be written as:

$$\rho_f S \frac{dp}{dt} + \nabla \cdot \left(\rho_f \left(-\frac{k_p}{\mu} \nabla \mathrm{p} \right) \right) + \rho_f \alpha \frac{d\varepsilon_v}{dt} = Q_f, \quad (1)$$

where ρ_f is the fluid density, S is the storage model (written as $\mathrm{S} = (1-\alpha)(\alpha - n)c_b + c_f n$, where c_b is the compressibility of the bulk material, α is Biot's effective stress coefficient, c_f is the compressibility of the fluid, and n is the porosity), p is the change in pore water pressure, k_p is the permeability, μ is the fluid dynamic viscosity, ε_v is the volumetric strain, and Q_f is the sink/source term.

The governing equation for force equilibrium of solid mechanics and the stress–strain constitutive relationship with linear material properties can be written as:

$$\begin{cases} \sigma_{ij} - \alpha p I = 0 \\ \sigma_{ij} = \mathbb{C}_{ijkl} \varepsilon_{kl} \end{cases}, \quad (2)$$

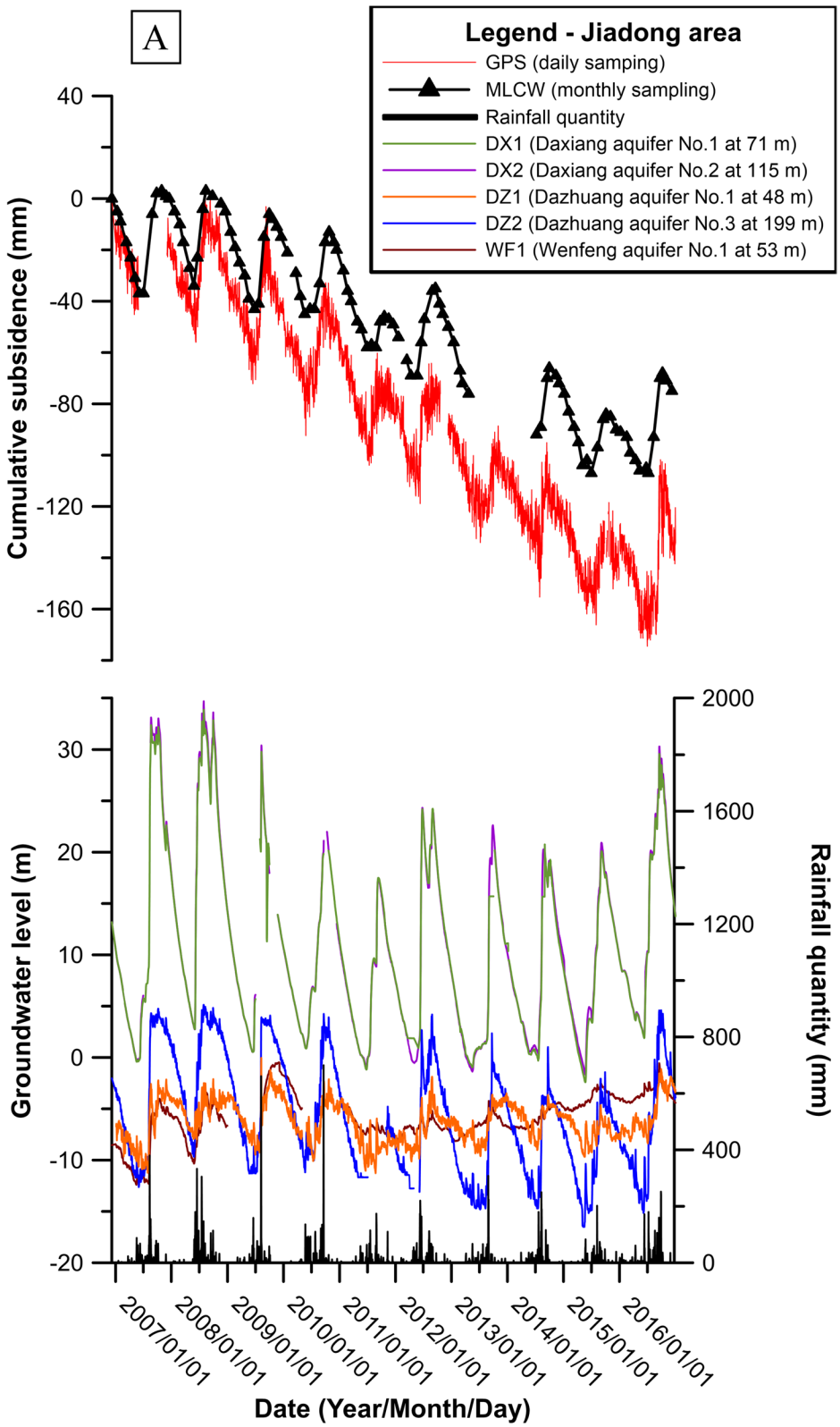

Fig. 3 Observation data for vertical displacement and groundwater levels in **A** Jiadong and **B** Fangliao areas. The MLCW data in the period 2013–2014 are missing. A negative (positive) value indicates the compression (expansion) of unconsolidated sediment

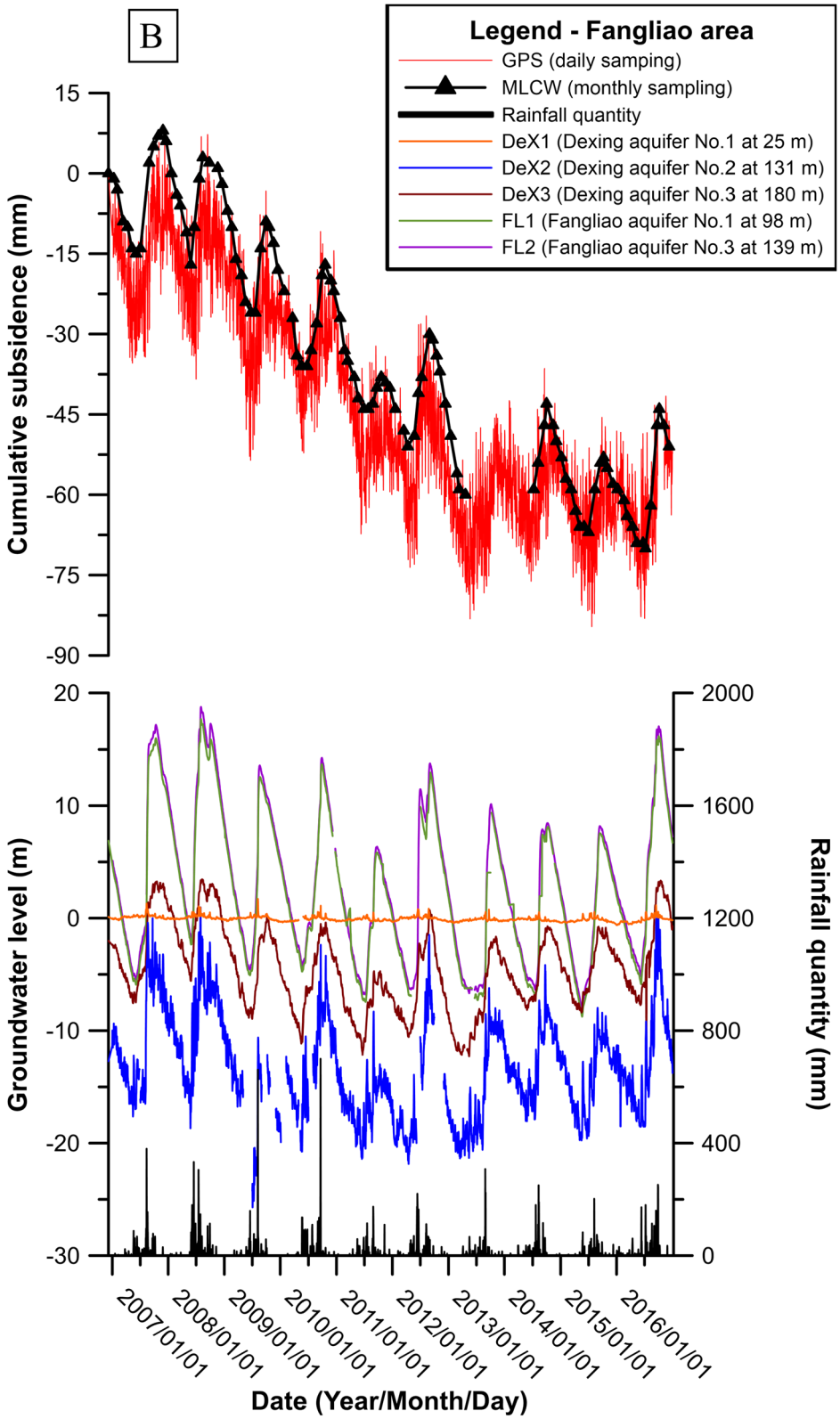

Fig. 3 continued

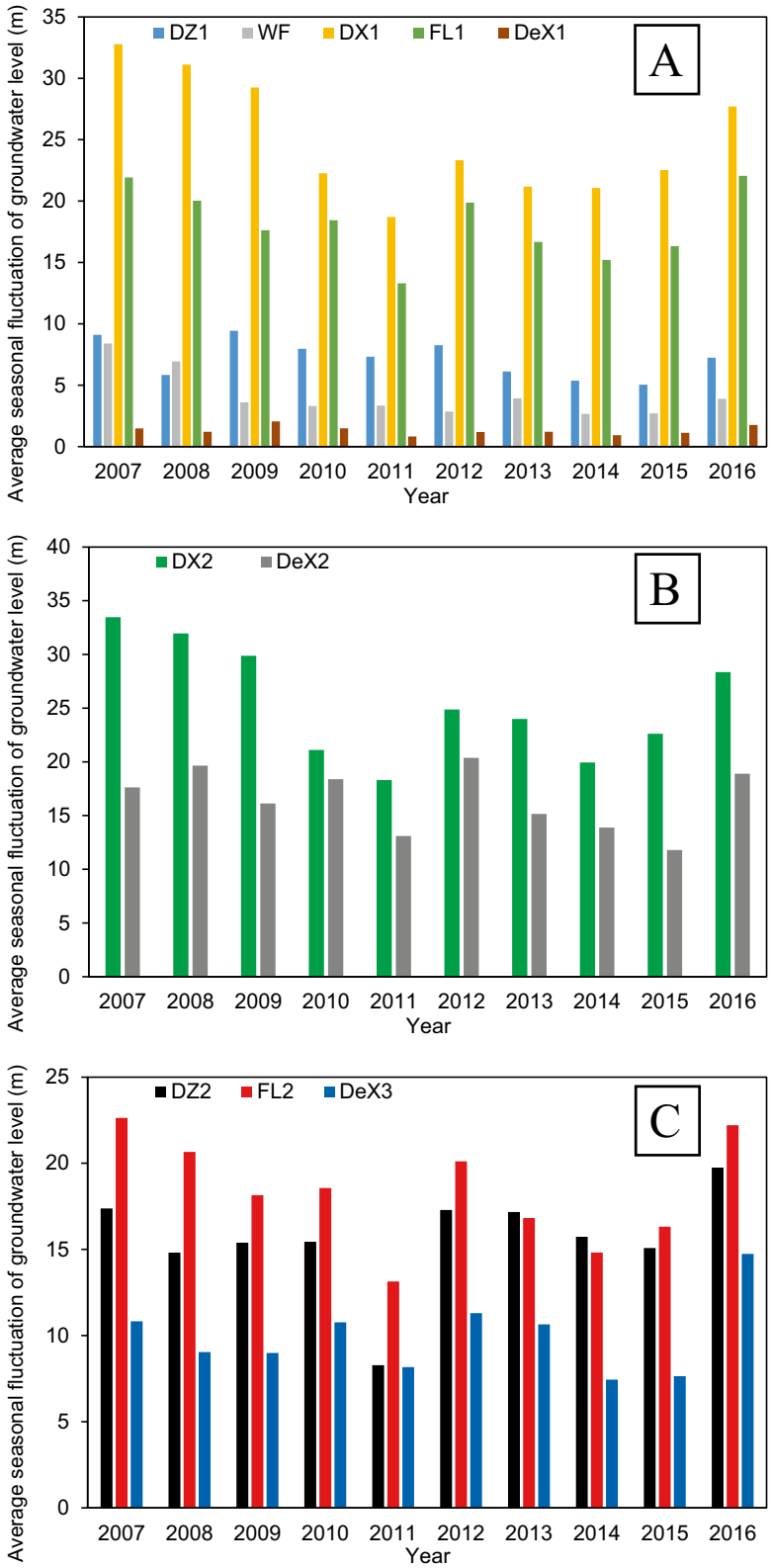

Fig. 4 Seasonal fluctuations of groundwater level in **A** first aquifer, **B** second aquifer, and **C** third aquifer. The abbreviations of monitoring wells are defined in Figs. 2 and 3

where σ_{ij} is the Cauchy stress tensor, I is the identity matrix, $\mathbb{C}_{ijkl}$ is the elastic matrix ($\mathbb{C}_{ijkl} = \frac{E\upsilon}{(1+\upsilon)(1-2\upsilon)} \delta_{ij}\delta_{kl} + \frac{E}{2(1+\upsilon)}(\delta_{ik}\delta_{jl} + \delta_{il}\delta_{jk})$, where E is Young's modulus, υ is Poisson's ratio, and $\delta_{ij} = \begin{cases} 1, i = j \\ 0, i \neq j \end{cases}$ is Kronecker's delta), and ε_{kl} is the Cauchy strain tensor. The strain ε_{ij} can be expressed as:

$$\varepsilon_{ij} = \frac{1}{2}\left(\nabla u + (\nabla u)^T\right), \tag{3}$$

where ∇u is the displacement gradient tensor and T denotes the transpose of the matrix.

To demonstrate the mechanism of hydraulic expansion and contraction, a simplified hydrogeological profile based on the Fangliao MLCW was developed, as shown in Fig. 5. According to the geological setting in the Fangliao area, three aquifers and three aquitards were set within a depth of 200 m. The bottom layer (aquitard 3) is considered to demonstrate deep displacement caused by hydraulic loading and unloading. The central column, with a width of 100 m, was the main area used to simulate hydraulic expansion and contraction. The boundary of the two sides of the hydrogeological profile was set to have no horizontal deformation and zero change in pore water pressure. To mitigate the boundary effect on the main area, the modeling domain was extended to 2.5 km away from the central column. The bottom boundary was set as a no-flow boundary with zero (fixed) displacement. The top boundary was set to have zero change in pore water pressure and the free-traction condition. A negative (positive) displacement indicates a downward (upward) movement or a compression (dilation) of strata. Six observation points in the central column (marked in Fig. 5) were chosen to demonstrate the simulation results.

The setting parameters and inverted results are listed in Table 1. Note that not all the values of these parameters are from experiments; some were obtained from the literature and model inversion because most of the required parameters are unavailable, especially the properties of the aquitard.

The initial condition is assumed to be the steady-state condition with zero change in pore water pressure and no displacement in the whole domain. Thus, a positive (negative) change in hydraulic head represents the hydraulic head being higher (lower) than the initial value. The sink and source due to seasonal variations are the driving force in the numerical model. Twelve months with seasonal variation, namely January to April (dry season), May to October (wet season), and November and

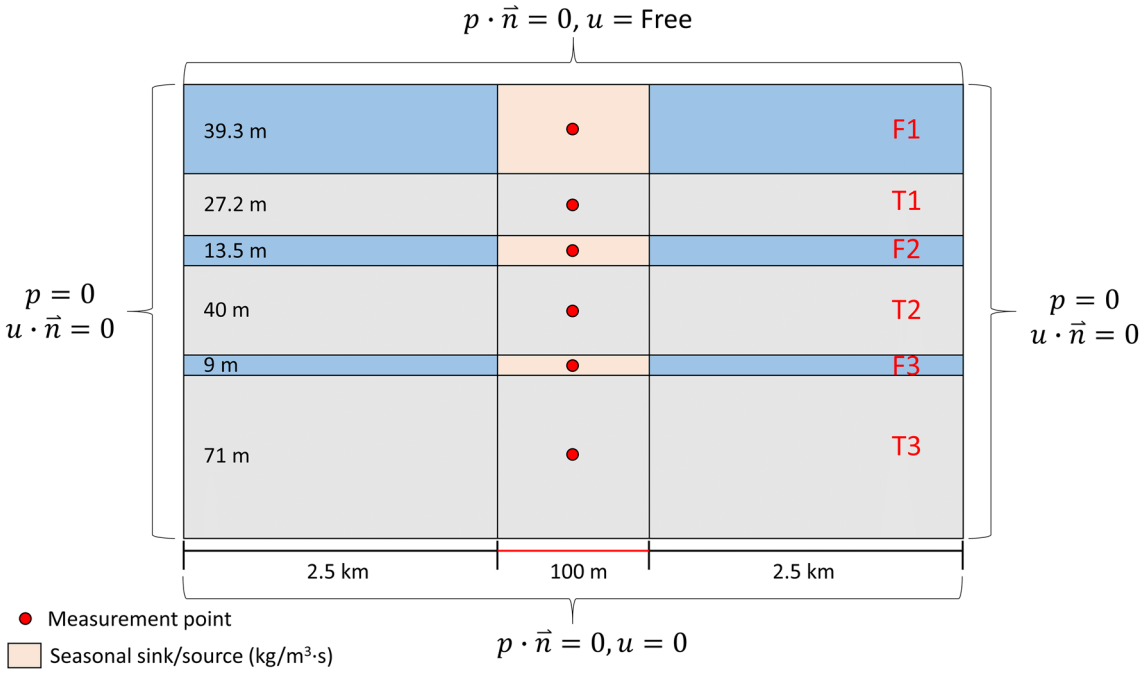

Fig. 5 Model diagram and boundary settings in hydromechanical model. F1, F2, and F3 indicate aquifer 1, aquifer 2, and aquifer 3, respectively, and T1, T2, and T3 indicate aquitard 1, aquitard 2, and aquitard 3, respectively. $\boldsymbol{u} \cdot \vec{\boldsymbol{n}} = 0$ is the no-deformation condition and $\boldsymbol{p} \cdot \vec{\boldsymbol{n}} = 0$ is the no-flow condition with normal vector $\vec{\boldsymbol{n}}$

Table 1 Material properties for hydromechanical model

Property type	Factors	Aquifer 1	Aquifer 2	Aquifer 3	Aquitard 1	Aquitard 2	Aquitard 3
Geometry	Width (m)	100	100	100	100	100	100
	Thickness (m)	39.3	13.5	9	27.2	40	62.3
Geological material properties	Porosity	0.3	0.35	0.3	0.4	0.3	0.4
	Permeability (m^2)	1.42×10^{-11}	1.36×10^{-12}	1.56×10^{-13}	7.09×10^{-16}	3.40×10^{-16}	7.50×10^{-17}
	Young's modulus (Pa)	1.96×10^{8}	5.64×10^{8}	1.96×10^{9}	2.31×10^{7}	2.64×10^{7}	4.56×10^{7}
	Poisson ratio	0.25	0.25	0.3	0.4	0.45	0.4
	Density (kg/m^3)	1600	1600	1600	1440	1440	1440
	Biot's coefficient	1	1	1	1	1	1
Fluid properties	Compressibility of fluid (1/Pa)			4.44×10^{-10}			
	Density (kg/m^3)			1000			
	Viscosity (Pa·s)			8.93×10^{-4}			

December (dry season), based on the hydrological conditions of the DeX groundwater observation were used to simulate the hydraulic expansion and contraction. In the dry (wet) season, the hydraulic head decreases (increases) due to groundwater discharge (recharge). Aquifer 1 is an unconfined aquifer and thus the change in hydraulic head is smaller than those for aquifers 2 and 3, which are confined aquifers.

Results

Data analysis

The rainfall quantities are not uniformly distributed in southern Taiwan. Annual rainfall is approximately 2380 mm, 95% of which is in the wet season. Groundwater level in the study area varies largely between the wet and dry seasons and induces an obvious variation of surface displacement (Figs. 3 and 4). In the wet season, the annual expansion of unconsolidated sediment at a shallow depth is 19.1 and 11.3 mm in the Jiadong and Fangliao areas, respectively, and the annual compression in the dry season is − 24.5 and − 16.5 mm in these areas, respectively. The compression over time in the Fangliao area showed a gradual decrease in subsidence rate after 2013, but the subsidence rate remained stable in the Jiadong area. The difference between the two areas may be attributed to differences in hydrogeological material deposition in different regions of the alluvial fan and differences in the compression stage of soil, including the time-delay phenomenon of clay compression. Land subsidence occurs in the dry season but rebounds in the wet season, which is consistent with the rainfall quantities. The rebound of shallow strata in the wet season is less than the compression in the dry season, leading to a long-term subsidence trend, which has been reported to be mainly due to groundwater over-extraction (Hung et al. 2010, 2018). The long-term shallow compression rates calculated from the MLCW data are − 9.7 and − 6.7 mm/yr in the Jiadong and Fangliao areas, respectively.

Correlation analyses

The calculated correlation coefficients between observation data are listed in Table 2. Time lag was not obvious in the correlation calculations and is thus not shown here. The correlation coefficients between the MLCW data and groundwater levels at different wells are high. Because this area is subjected to serious groundwater extraction, the high correlation implies that the shallow compression is mainly due to groundwater over-extraction induced by anthropogenic activity. The correlation coefficients between groundwater levels at different depths at a given location are high, which indicates that the variation patterns at different depths are consistent due to groundwater discharge in the dry season and rainfall recharge in the wet season. Fourier analysis shows that all these data have predominant periods of about 1 year. Therefore, the rainfall, shallow groundwater level, deep groundwater level, and MLCW observations indicate that the driving forces of the variations in these time series are the same. However, after the removal of shallow compression, the correlation coefficients between deep displacement and other observations become very small and even negative, which implies that the mechanism of deep displacement is different from that of shallow compression.

Deep displacement

Figure 6A and B shows the calculation results of deep displacement in the Jiadong and Fangliao areas, respectively, along with shallow compression and rainfall quantities.

Table 2 Correlation coefficients for various components

	CLON GPS	Jiadong MLCW	JD-DD	DZ1	DZ2	WF	DX1	DX2	FL1	FL2	DeX1	DeX2	DeX3	CRD
FALI GPS	0.71	–	–	0.69	0.71	0.58	0.64	0.64	0.73	0.73	-0.06	0.72	0.82	0.10
Fangliao MLCW	–	0.95	–	0.84	0.91	0.58	0.84	0.84	0.92	0.92	0.17	0.90	0.95	0.35
FL-DD	–	–	0.42	− 0.25	− 0.37	− 0.02	− 0.35	− 0.33	− 0.37	− 0.35	− 0.32	− 0.32	− 0.24	− 0.47
DZ1	0.74	0.84	− 0.18	1.00	0.87	0.66	0.68	0.67	0.78	0.78	0.17	0.73	0.74	0.47
DZ2	0.90	0.91	− 0.03	0.87	1.00	0.63	0.93	0.92	0.98	0.97	0.27	0.87	0.87	0.60
WF	0.48	0.63	− 0.26	0.66	0.63	1.00	0.54	0.53	0.54	0.54	0.00	0.46	0.50	0.25
DX1	0.80	0.76	0.11	0.68	0.93	0.54	1.00	1.00	0.96	0.96	0.38	0.86	0.88	0.47
DX2	0.79	0.76	0.11	0.67	0.92	0.53	1.00	1.00	0.95	0.96	0.39	0.86	0.88	0.44
FL1	0.91	0.89	0.04	0.78	0.98	0.54	0.96	0.95	1.00	1.00	0.25	0.87	0.90	0.55
FL2	0.90	0.89	0.05	0.78	0.97	0.54	0.96	0.96	1.00	1.00	0.23	0.88	0.90	0.54
DeX1	0.09	0.01	0.16	0.17	0.27	0.00	0.38	0.39	0.25	0.23	1.00	0.34	0.30	0.09
DeX2	0.71	0.72	− 0.01	0.73	0.87	0.46	0.86	0.86	0.87	0.88	0.34	1.00	0.92	0.32
DeX3	0.72	0.70	0.06	0.74	0.87	0.50	0.88	0.88	0.90	0.90	0.30	0.92	1.00	0.25
CRD	0.65	0.72	− 0.10	0.47	0.60	0.25	0.47	0.44	0.55	0.54	0.09	0.32	0.25	1.00

JD-DD: deep displacement in Jiadong area; FL-DD: deep displacement in Fangliao area; CRD: cumulative rainfall departure. The abbreviations of monitoring wells are defined in Figs. 2 and 3. Note that this table is separated into two parts. The first three columns and rows assess the correlation between deformation in different areas with hydrological data; thus, the quantities are not symmetrical between columns and rows. The fourth to fourteenth columns and rows show the correlation between the hydrological data; thus, the quantities are symmetrical between columns and rows

The contribution of deep displacement to total land subsidence is 37.06% and 13.63% in the Jiadong and Fangliao areas, respectively (Fig. 7). The average rates of deep displacement are − 4.6 and 0.9 mm/yr in the Jiadong and Fangliao areas, respectively. Deep displacement in both areas shows fluctuation over time. The predominant periods are about 1 year, which might be related to the hydrological cycle. However, most of the correlation coefficients between groundwater level and deep displacement are low or even negative (Table 2). The calculated correlation coefficients between deep displacement and rainfall (calculated as cumulative rainfall departure; Weber and Stewart 2004) in the Fangliao and Jiadong areas are both negative (− 0.47 and − 0.10, respectively) and exhibit no time lag. Although the correlation of shallow compression between the Jiadong and Fangliao areas is high (0.95), the trends of deep displacement in these two areas are totally different; their correlation coefficient is only 0.42 (Table 2).

After the removal of shallow compression, the correlation coefficients between deep displacement and other observations become very small and even negative (Table 2), which implies that the mechanism of deep displacement is different from that of shallow compression. To understand the mechanism of deep displacement, the threshold between shallow and deep components was set to various depths. For each station, three depths were set as the threshold to calculate shallow compression and deep displacement. The MLCW data for depths of 47, 118, and 194 m in the Jiadong area and those for depths of 67, 121, and 191 m in the Fangliao area were selected based on the MLCW measurement depth and the hydrogeological model of the aquifer system in Pingtung Plain. For each depth, shallow compression was measured based on MLCW data from the land surface to the given depth and deep displacement was calculated based on the difference between GPS values and MLCW values. The results of cross-correlation are listed in Table 3. The time lag information calculated from cross-correlation is also shown in the table to demonstrate that the time lag is not obvious. It is interesting to see that the deep displacement at shallow depths has high correlations with hydrological observations but the quantities decrease with increasing depth. The results clearly show that at a certain depth, the correlation between deep displacement and hydrological observations transitions from positive to negative.

Discussion

The deep displacement (beyond a depth of 200 m) results in both areas fluctuate temporally, which might be related to the hydrological cycle. The mechanism of the variations of deep displacement could be cyclic hydraulic loading (e.g., Fu et al. 2012; Chanard et al. 2014; Martens 2016; Knappe et al. 2019; Hsu et al. 2020, 2021; Tran 2020), which induces the hydraulic expansion and contraction proposed in the present study (Fig. 8). Cyclic hydraulic loading is an additional form of seasonal loading and unloading and contributes to the total mass variations at a certain depth. An increase (decrease) in pore water pressure in the aquifer induces an expansion (contraction) condition that both uplifts (sinks) the top strata

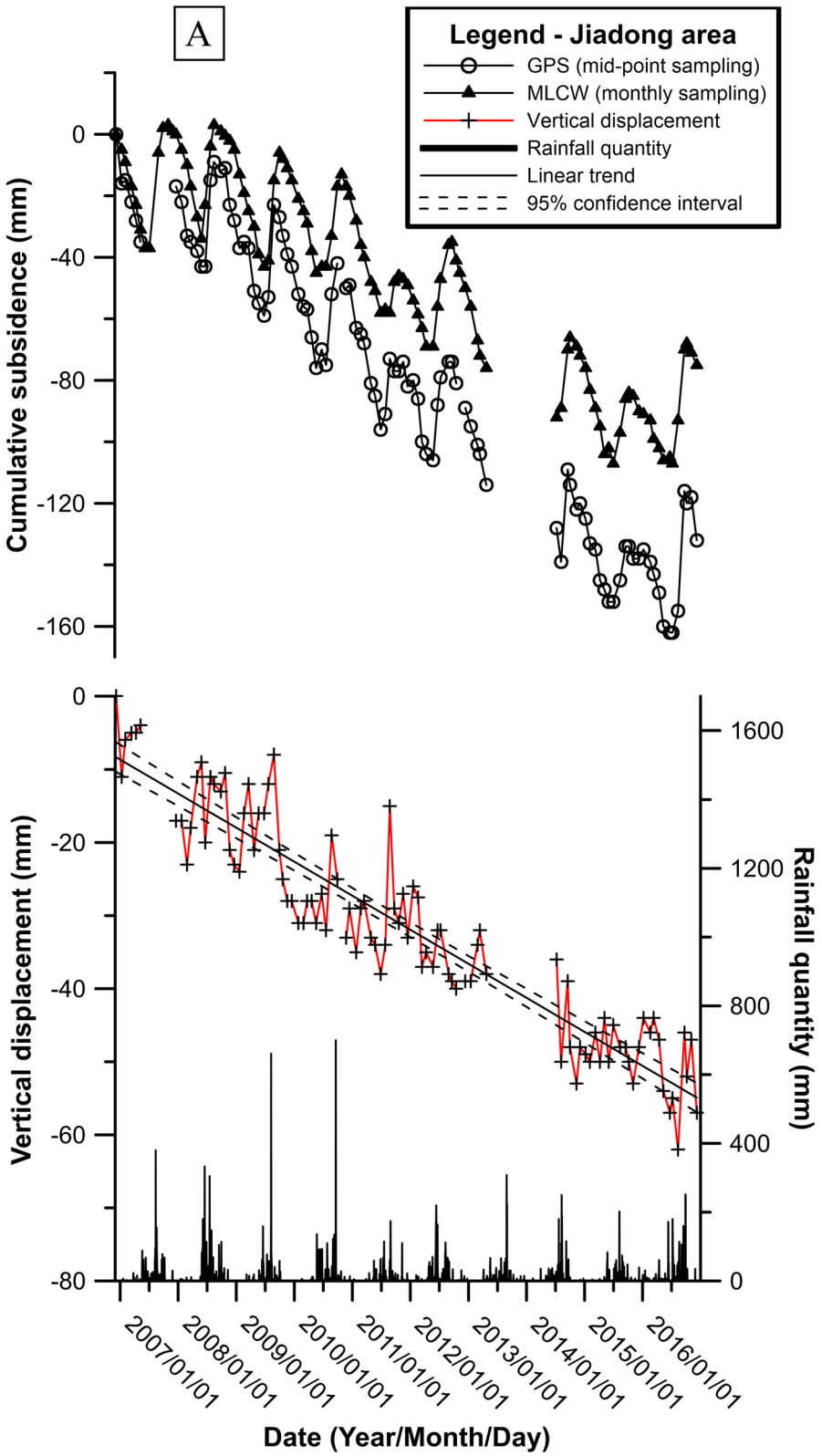

Fig. 6 Comparison between observed subsidence and calculated deep displacement with rainfall in **A** Jiadong area and **B** Fangliao area

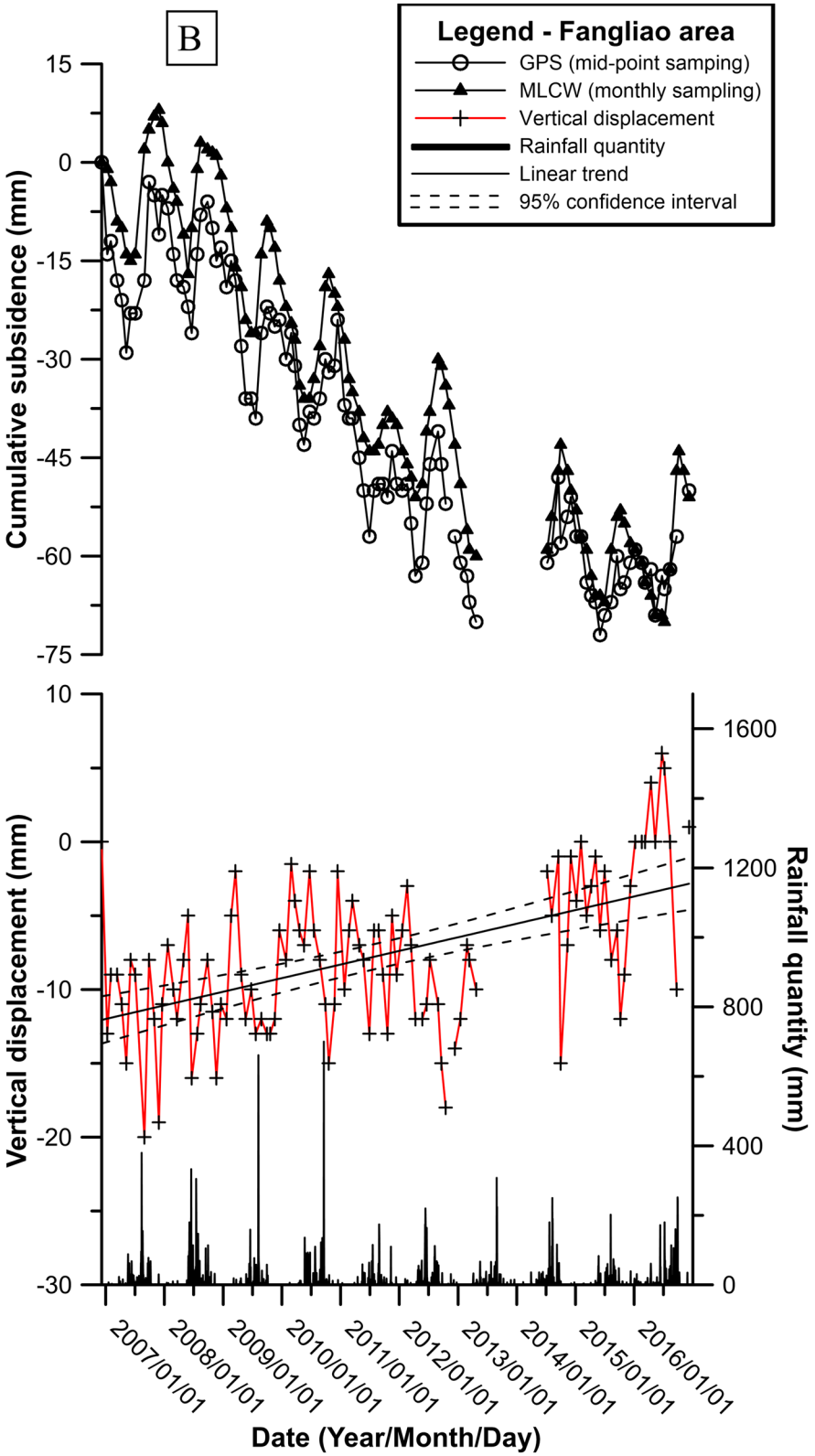

Fig. 6 continued

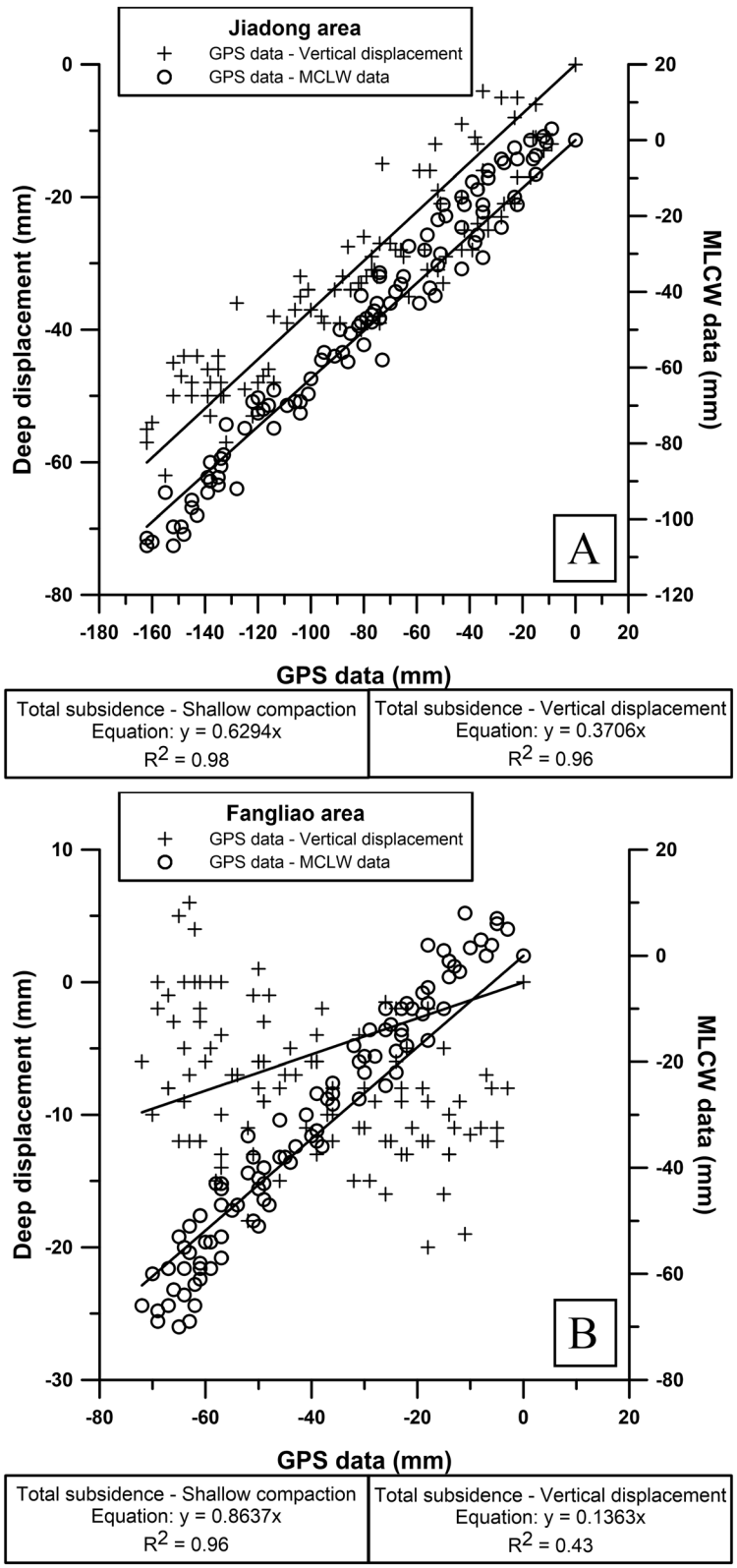

Fig. 7 Mean ratio of shallow compression and deep displacement to total subsidence in **A** Jiadong area and **B** Fangliao area

Table 3 Correlation coefficients for various deep displacement depths

Area	Condition	DZ1	DZ2	WF	DX1	DX2	FL1	FL2	DeX1	DeX2	DeX3	CRD
JD	Deep displacement below 47 m	0.59(0)	0.70(0)	0.34(0)	0.65(0)	0.62(0)	0.73(0)	0.74(0)	0.14(0)	0.55(0)	0.60(0)	0.56(0)
	Deep displacement below 118 m	0.16(− 1)	0.20(0)	0.04(− 1)	0.27(0)	0.28(0)	0.24(0)	0.26(0)	0.28(1)	0.18(− 1)	0.23(− 1)	0.16(− 1)
	Deep displacement below 194 m	− 0.18(0)	− 0.03(0)	− 0.26(0)	0.11(0)	0.11(0)	0.04(0)	0.05(0)	0.16(0)	− 0.01(0)	0.06(0)	− 0.10(0)
FL	Deep displacement below 67 m	0.60(0)	0.53(1)	0.52(0)	0.57(1)	0.56(1)	0.56(0)	0.57(0)	− 0.26(− 1)	0.57(0)	0.69(1)	0.02(0)
	Deep displacement below 121 m	0.37(1)	0.28(1)	0.43(1)	0.30(1)	0.28(1)	0.29(1)	0.30(1)	− 0.20(− 1)	0.33(1)	0.45(1)	− 0.28(− 1)
	Deep displacement below 191 m	− 0.25(0)	− 0.37(0)	− 0.02(0)	− 0.35(0)	− 0.33(0)	− 0.37(0)	− 0.35(0)	− 0.32(0)	− 0.32(0)	− 0.24(0)	− 0.47(0)

JD Jiadong area, *FL* Fangliao area, *CRD* cumulative rainfall departure. The values in brackets indicates the time lag in months. Positive (negative) values indicate that row factor is faster (slower) than column factor. The abbreviations of monitoring wells are defined in Figs. 2 and 3

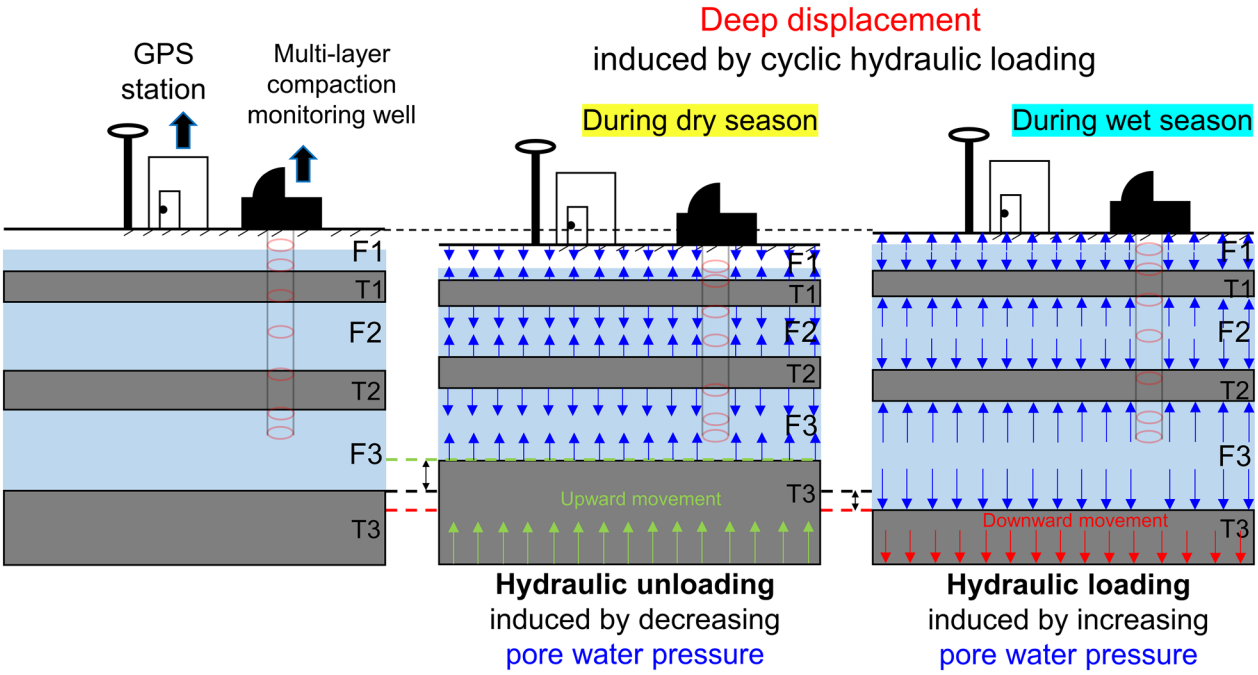

Fig. 8 Conceptual model of deep displacement induced by hydraulic loading and unloading. Downward (upward) movement of deep strata is related to hydraulic loading (unloading) during wet (dry) season

and loads (unloads) the bottom strata. The effect of an increase in pore water pressure on the top strata is an uplift of the ground surface and that on the bottom strata is hydraulic loading.

The groundwater level in the wet season at a deep aquifer (e.g., DZ2, DeX3, or FL2) can increase pore water pressure at a depth of 200 m (Fig. 4C), which is large enough to create observable hydraulic loading on strata deeper than 200 m. A negative (positive) value of annual displacement indicates the downward (upward) movement of deep strata due to increasing (decreasing) pore water pressure. Figure 9 shows the phenomenon of cyclic hydraulic loading and unloading. In Fig. 9A, detrended deep displacement and detrended hydraulic factors show an obviously negative relationship in the Fangliao area. In Fig. 9B, during the wet season, the average downward displacements are − 1.6 and − 14.6 mm/yr in the Jiadong and Fangliao areas, respectively, and during the dry season, the average uplift displacements are 5.9 and 12.6 mm/yr in these areas, respectively. Cyclic hydraulic loading and unloading are obvious in the Fangliao area but not in the Jiadong area,

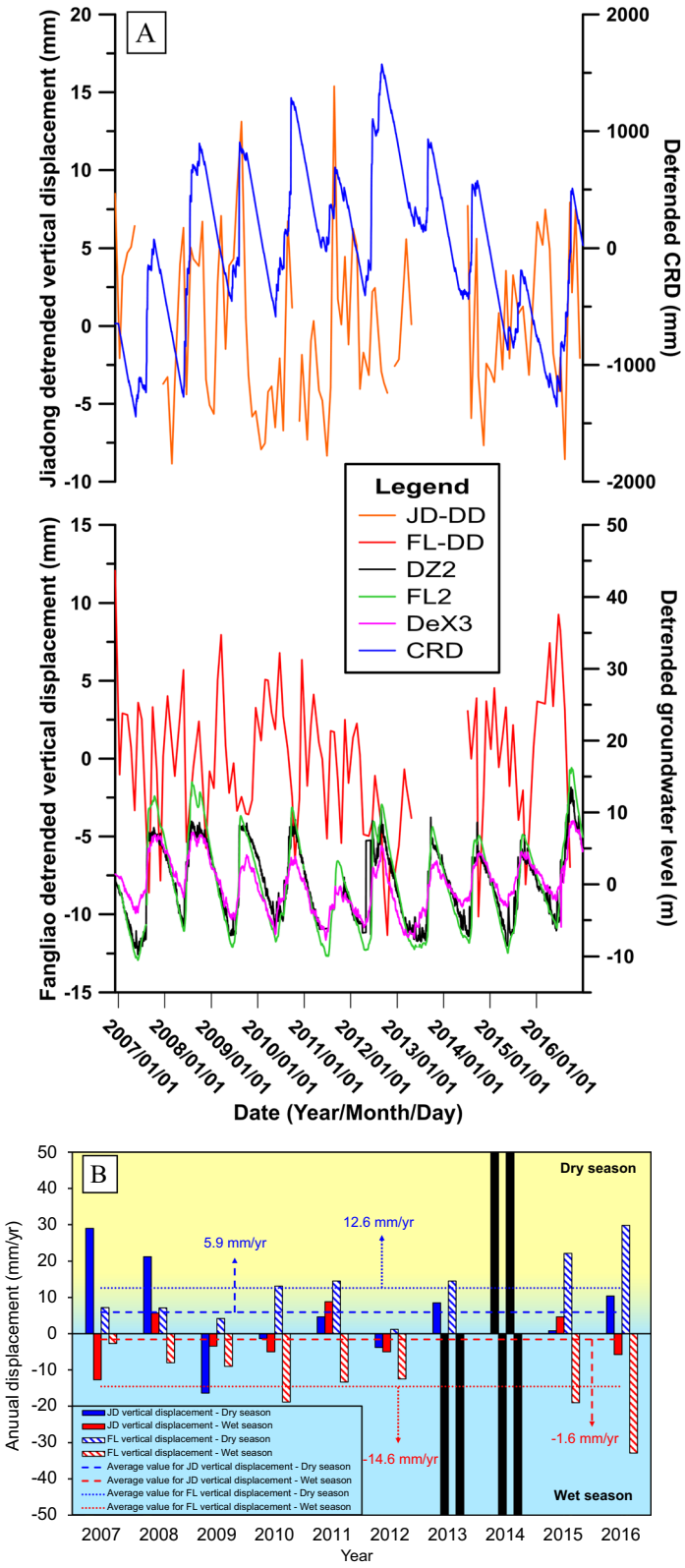

Fig. 9 **A** Time series comparison between deep displacements and hydrological observations. Note that the time series are detrended results. **B** Seasonal variations of deep displacement and cyclic hydraulic loading. The black columns mark the missing data of MLCWs. The abbreviations of monitoring wells are defined in Figs. 2 and 3. CRD: cumulative rainfall departure

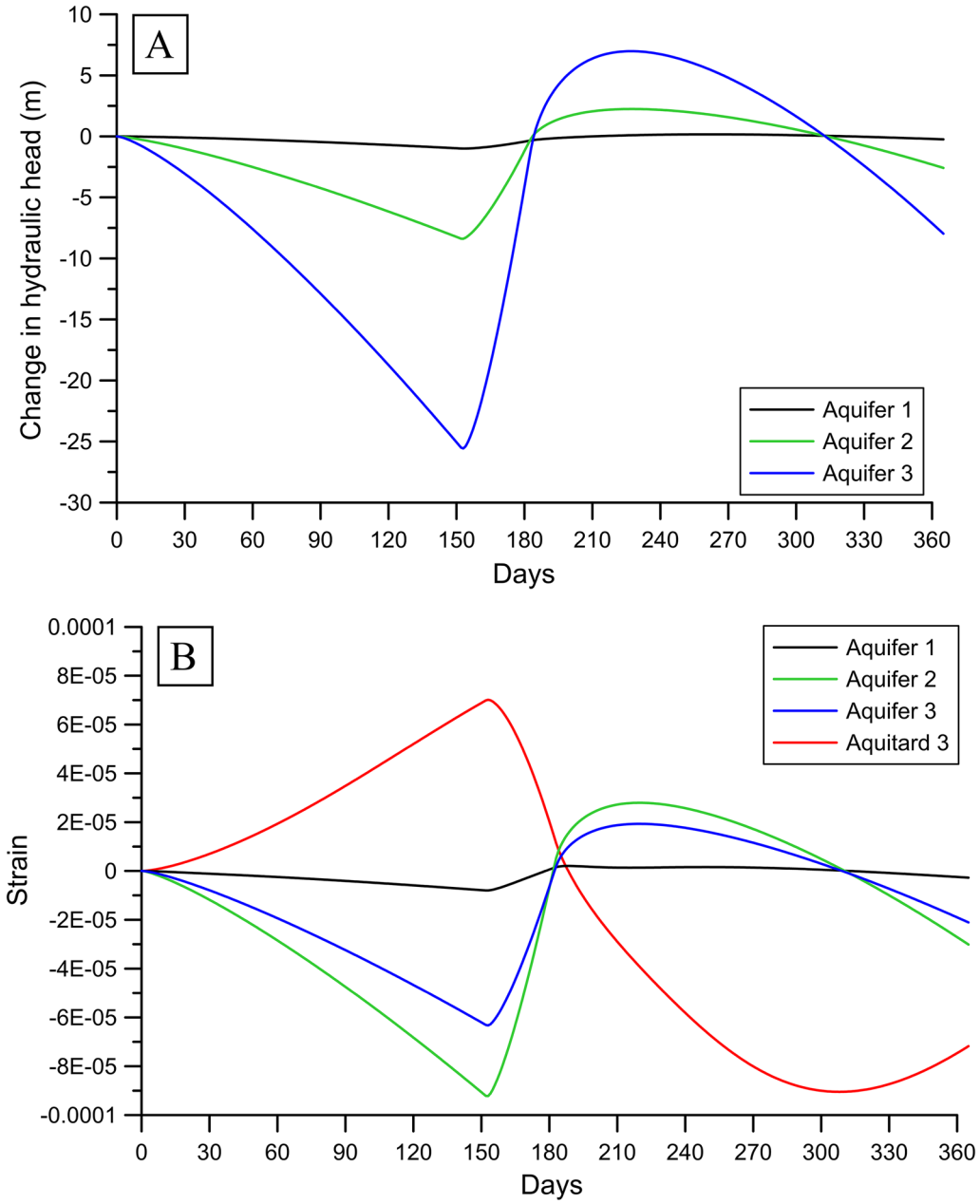

Fig. 10 Simulated **A** change in pore water pressure in three aquifers and **B** strain in three aquifers and aquitard 3 (i.e., bottom layer)

which might be due to the observation stations not being collocated in the Jiadong area (Fig. 1B) or due to differences in their hydrogeological properties.

Note that the observation of vertical displacement on the ground surface in the wet and dry seasons shows uplift and decline, respectively, due to rainfall recharge and groundwater discharge. After the removal of shallow compression, the deep vertical displacement in the wet and dry seasons shows decline and uplift, respectively. Deep displacement variations are opposite to surface displacement variations. The hydraulic expansion and contraction can well explain the observations. The opposite responses indicate that the effects of natural factors (such as tectonic activity, plate displacement, and hydraulic loading) obtained without the removal of the influence of anthropogenic activity will lead to large uncertainty in the assessment results. The negative correlation between hydrological data and deep displacement shown in this study is similar to the concept of cyclic hydrological loading, proposed by Hsu et al.

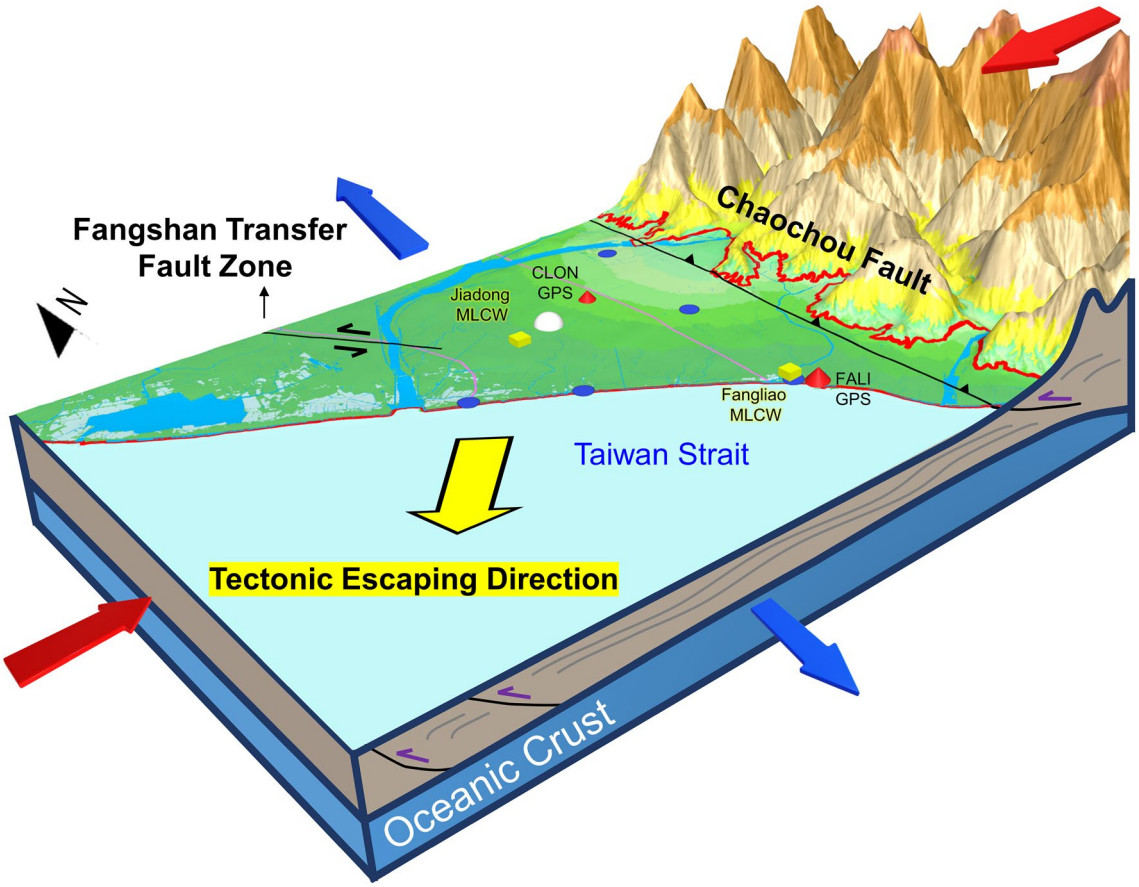

Fig. 11 Three-dimensional diagram of tectonic activity (after Chiang 1971; Lacombe et al. 2001; Hou et al. 2005; Hu et al. 2006, 2007; Ching et al. 2007). The observation stations correspond to those in Fig. 1

(2021), who used surface deformation (Global Navigation Satellite System data) along with rainfall and groundwater data in Taiwan to study the hydraulic variations that trigger earthquakes. Their results indicated that seasonal groundwater level variations could be an important trigger of earthquakes. The phenomenon of hydraulic expansion and contraction in deep strata proposed here supports their speculation.

A coupled hydromechanical model is used to demonstrate the phenomenon of hydraulic expansion and contraction. The simulation results are shown in Fig. 10. The phenomenon of hydraulic expansion and contraction can be demonstrated by the simulated strain in the developed hydromechanical model. The simulated strain in aquifers 1 to 3 shows a decreasing trend (compression) in the dry season and an increasing trend (dilation) in the wet season, which is consistent with observations. However, the simulated strain in aquitard 3 shows the opposite responses, that is, an increasing trend (dilation) in the dry season and a decreasing trend (compression) in the wet season. This reversed phenomenon is the cyclic hydraulic expansion and contraction in the aquifer system proposed in this study. Note that this phenomenon only occurs when the formation has a small permeability (Table 1). Such conditions include, for example, the presence of an aquitard capable of forming an interface to absorb stress caused by variations in pore water pressure within an adjacent aquifer. Consequently, the occurrence of hydraulic expansion and contraction is contingent upon the strata meeting specific criteria, such as possessing a very small permeability at certain depths. The findings from the hydromechanical simulations corroborate observed behaviors and support the mechanism proposed in this study.

The linear trend of deep displacement in Fig. 6 might be due to tectonic activity, as discussed in the literature (e.g., Kuo et al. 2001; Hou et al. 2005; Hu et al. 2006, 2007). Figure 11 shows that the direction of tectonic escape is toward the southwest, with an azimuth that ranges from 243.9° to 245.7° (Tran and Wang 2020). In this study, an average horizontal displacement rate of 26.6 mm/yr was calculated using GPS data; this value is consistent with

the findings of Hu et al. (2006). Furthermore, Hu et al. (2007) found that a tectonic escape connected with a tectonic extrusion and a lateral extrusion operates at the southern tip of the Taiwan collision belt. It is thus important to recognize that the horizontal displacement of a stratum corresponds to its vertical displacement since the extension and contraction of the stratum can also change its thickness or elevation (Hu et al. 2007). However, since there is no further evidence to support the mechanism of the linear trend of deep displacement, it is not discussed in this study.

Conclusions

GPS, MLCW, rainfall, and groundwater level data were collected to investigate the mechanism of deep vertical displacement in Pingtung Plain, Taiwan, which is located in a tectonically active coastal area. The collected data all showed obvious seasonal variations with a predominant period of about 1 year. The variations of deep displacement also have a 1-year period but are opposite to those of hydrological data, indicating that these variations are likely due to cyclic hydraulic loading and unloading. The large variations of groundwater level at a depth of 200 m create cyclic hydraulic loading and unloading for strata at depths deeper than 200 m, which explains the variations of deep displacement. The correlation coefficients between hydrological data and deep displacement at various depths show a decrease with depth (without obvious time lag), from a high positive correlation to a negative correlation. The results imply that the phenomenon of hydraulic expansion and contraction can be observed at certain depths. A simulation using a coupled hydromechanical model was conducted. The simulation results demonstrate that the phenomenon of hydraulic expansion and contraction may occur when a deep formation has a small permeability. The numerical model results are consistent with the observations and the proposed mechanism. In the Jiadong and Fangliao areas, deep displacement contributes 37.06% and 13.63% to total subsidence, respectively. These contributions are similar to that for tectonic activity estimated in the literature for the study area, indicating that the linear trend of deep displacement might be due to tectonic activity. However, there is no evidence to support this mechanism; further investigations are thus needed.

The variations of deep vertical displacement are opposite to those of ground surface vertical displacement. The opposite responses indicate that the effects of natural factors on the ground surface obtained without the removal of the influence of anthropogenic activity will lead to large uncertainty in the assessment results. The study results provide important information on the mechanism of deep vertical displacement, which support the suggestion, proposed in the literature, that groundwater level variations might trigger earthquakes. This study provides partial evidence for the mechanism of deep vertical displacement. Further observations and investigations are required to provide more evidence.

Acknowledgements
The authors would like to thank Professor Jyr-Ching Hu at National Taiwan University and Dr. Wei-Chia Hung at Green Environmental Engineering Consultant Co. Ltd. for their consultation regarding the tectonic system and subsidence observations.

Author contributions
Duc-Huy Tran: data curation, formal analysis, methodology, software, investigation, writing—original draft, discussion. Shih-Jung Wang: conceptualization, methodology, writing—review and editing, validation, discussion, supervision. Jian-Yu Chen: software, discussion.

Funding
This study was funded by the Ministry of Science and Technology, Taiwan (MOST), under grants MOST 108–2638-E-008–001-MY2, MOST 109–2116-M-008–016, MOST 110–2123-M-008–001, and MOST 111–2116-M-008–007, the National Science and Technology Council, Taiwan (NSTC), under grants NSTC 111–2123-M-008–001, NSTC 112–2116-M-008–004, and NSTC 112–2123-M-008–001, and the Water Resources Agency, Taiwan (WRA), under grants MOEAWRA 1100304 and MOEAWRA 1110346.

Data availability
The GPS and hydrology data adopted in this study can be obtained from the website of Academia Sinica (https://tgm.earth.sinica.edu.tw/) and the Water Resources Agency, Taiwan (https://gweb.wra.gov.tw/wrhygis/), respectively. The website for hydrology data is mainly in Chinese. To convert years in the Republic of China calendar to years in the Gregorian calendar, add 1911 years. For example, the year 109 in the Republic of China calendar is the year 2020 (109 + 1911) in the Gregorian calendar. Clicking on a year opens a page that includes the text "Hydrological Year Book". Clicking on this text opens the data page. The adopted data are from a file with rainfall and groundwater data. Note that the Water Resources Agency has not yet released the raw data of multi-layer compaction monitoring wells for public use.

Declarations

Competing interests
The authors declare that they have no conflicts of interest.

Author details
[1]Graduate Institute of Applied Geology, National Central University, 300 Zhongda Rd., Zhongli District, Taoyuan City 32001, Taiwan. [2]Department of Earth Sciences, National Central University, 300 Zhongda Rd., Zhongli District, Taoyuan City 32001, Taiwan.

Received: 19 October 2023 Accepted: 29 April 2024
Published online: 15 May 2024

References

Alley WM, Healy RW, LaBaugh JW, Reilly TE (2002) Flow and storage in groundwater systems. Science 296:1985–1990. https://doi.org/10.1126/science.1067123

Bos AG, Spakman W, Nyst MC (2003) Surface deformation and tectonic setting of Taiwan inferred from a GPS velocity field. J Geophys Res Solid Earth.108. https://doi.org/10.1029/2002JB002336

Carminati E, Di Donato G (1999) Separating natural and anthropogenic vertical movements in fast subsiding areas: the Po plain (N. Italy) case. Geophys Res Lett 26:2291–2294

Chanard K, Avouac J, Ramillien G, Genrich J (2014) Modeling deformation induced by seasonal variations of continental water in the Himalaya

region: sensitivity to Earth elastic structure. J Geophys Res Solid Earth 119:5097–5113. https://doi.org/10.1002/2013JB010451
Chen C-T, Kuo C-H, Lin C-M, Huang J-Y, Wen K-L (2022) Investigation of shallow S-wave velocity structure and site response parameters in Taiwan by using high-density microtremor measurements. Eng Geol 106498. https://doi.org/10.1016/j.enggeo.2021.106498
Chiang S (1971) Seismic study of the Chaochou structure, Pingtung, Taiwan. Petrol Geol Taiwan 8:281–294
Chiang CS, Yu HS, Chou YW (2004) Characteristics of the wedge-top depozone of the southern Taiwan foreland basin system. Basin Res 16:65–78. https://doi.org/10.1111/j.1365-2117.2004.00222.x
Ching K-E, Rau R-J, Lee J-C, Hu J-C (2007) Contemporary deformation of tectonic escape in SW Taiwan from GPS observations, 1995–2005. Earth Planet Sci Lett 262:601–619. https://doi.org/10.1016/j.epsl.2007.08.017
Ching KE, Hsieh ML, Johnson KM, Chen KH, Rau RJ, Yang M (2011) Modern vertical deformation rates and mountain building in Taiwan from precise leveling and continuous GPS observations, 2000–2008. J Geophys Res Solid Earth 116. https://doi.org/10.1029/2011JB008242
Erban LE, Gorelick SM, Zebker HA, Fendorf S (2013) Release of arsenic to deep groundwater in the Mekong Delta, Vietnam, linked to pumping-induced land subsidence. Proc Natl Acad Sci 110:13751–13756. https://doi.org/10.1073/pnas.1300503110
Fu Y, Freymueller JT, Jensen T (2012) Seasonal hydrological loading in southern Alaska observed by GPS and GRACE. Geophys Res Lett 39. https://doi.org/10.1029/2012GL052453
Galloway DL, Burbey TJ (2011) Regional land subsidence accompanying groundwater extraction. Hydrogeol J 19:1459–1486. https://doi.org/10.1007/s10040-011-0775-5
Galloway DL, Hudnut KW, Ingebritsen S, Phillips SP, Peltzer G, Rogez F, Rosen P (1998) Detection of aquifer system compaction and land subsidence using interferometric synthetic aperture radar, Antelope Valley, Mojave Desert, California. Water Resour Res 34:2573–2585. https://doi.org/10.1029/98WR01285
Gambolati G, Teatini P, Ferronato M (2006) Anthropogenic land subsidence. Encycl Hydrol Sci. https://doi.org/10.1002/0470848944.hsa164b
Hou C-S, Hu J-C, Shen L-C, Wang J-S, Chen C-L, Lai T-C, Huang C, Yang Y-R, Chen R-F, Chen Y-G (2005) Estimation of subsidence using GPS measurements, and related hazard: the Pingtung Plain, southwestern Taiwan. C R Geosci 337:1184–1193. https://doi.org/10.1016/j.crte.2005.05.012
Hsieh C-S, Shih T-Y, Hu J-C, Tung H, Huang M-H, Angelier J (2011) Using differential SAR interferometry to map land subsidence: a case study in the Pingtung Plain of SW Taiwan. Nat Hazards 58:1311–1332. https://doi.org/10.1007/s11069-011-9734-7
Hsu K-C, Wang C-H, Chen K-C, Chen C-T, Ma K-W (2007) Climate-induced hydrological impacts on the groundwater system of the Pingtung Plain, Taiwan. Hydrogeol J 15:903–913. https://doi.org/10.1007/s10040-006-0137-x
Hsu Y-J, Fu Y, Bürgmann R, Hsu S-Y, Lin C-C, Tang C-H, Wu Y-M (2020) Assessing seasonal and interannual water storage variations in Taiwan using geodetic and hydrological data. Earth Planet Sci Lett 550:116532. https://doi.org/10.1016/j.epsl.2020.116532
Hsu Y-J, Kao H, Bürgmann R, Lee Y-T, Huang H-H, Hsu Y-F, Wu Y-M, Zhuang J (2021) Synchronized and asynchronous modulation of seismicity by hydrological loading: a case study in Taiwan. Sci Adv 7:eabf7282. https://doi.org/10.1126/sciadv.abf7282
Hu J-C, Chu H-T, Hou C-S, Lai T-H, Chen R-F, Nien P-F (2006) The contribution to tectonic subsidence by groundwater abstraction in the Pingtung area, southwestern Taiwan as determined by GPS measurements. Quat Int 147:62–69. https://doi.org/10.1016/j.quaint.2005.09.007
Hu J-C, Hou C-S, Shen L-C, Chan Y-C, Chen R-F, Huang C, Rau R-J, Chen KH-H, Lin C-W, Huang M-H (2007) Fault activity and lateral extrusion inferred from velocity field revealed by GPS measurements in the Pingtung area of southwestern Taiwan. J Asian Earth Sci 31:287–302. https://doi.org/10.1016/j.jseaes.2006.07.020
Hung W-C, Hwang C, Chang C-P, Yen J-Y, Liu C-H, Yang W-H (2010) Monitoring severe aquifer-system compaction and land subsidence in Taiwan using multiple sensors: Yunlin, the southern Choushui River Alluvial Fan. Environ Earth Sci 59:1535–1548. https://doi.org/10.1007/s12665-009-0139-9
Hung W-C, Hwang C, Chen Y-A, Zhang L, Chen K-H, Wei S-H, Huang D-R, Lin S-H (2018) Land subsidence in Chiayi, Taiwan, from compaction well, leveling and alos/palsar: aquaculture-induced relative sea level rise. Remote Sens 10:40. https://doi.org/10.3390/rs10010040
Hung W-C, Hwang C, Sneed M, Chen YA, Chu CH, Lin SH (2021) Measuring and interpreting multilayer aquifer-system compactions for a sustainable groundwater-system development. Water Resour Res 57. https://doi.org/10.1029/2020WR028194
Hwang C, Yang Y, Kao R, Han J, Shum C, Galloway DL, Sneed M, Hung W-C, Cheng Y-S, Li F (2016) Time-varying land subsidence detected by radar altimetry: California, Taiwan and north China. Sci Rep 6:1–12. https://doi.org/10.1038/srep28160
Jankowski KL, Törnqvist TE, Fernandes AM (2017) Vulnerability of Louisiana's coastal wetlands to present-day rates of relative sea-level rise. Nat Commun 8:1–7. https://doi.org/10.1038/ncomms14792
Jones CE, An K, Blom RG, Kent JD, Ivins ER, Bekaert D (2016) Anthropogenic and geologic influences on subsidence in the vicinity of New Orleans, Louisiana. J Geophys Res Solid Earth 121:3867–3887. https://doi.org/10.1002/2015JB012636
Knappe E, Bendick R, Martens H, Argus D, Gardner W (2019) Downscaling vertical GPS observations to derive watershed-scale hydrologic loading in the northern Rockies. Water Resour Res 55:391–401. https://doi.org/10.1029/2018WR023289
Kuo C, Chan C, Wang C (2001) Subsidence (-) over withdrawal groundwater, tectonic or both? AGUFM 2001:H42D-0401
Kuo C-H, Chen C-T, Lin C-M, Wen K-L, Huang J-Y, Chang S-C (2016) S-wave velocity structure and site effect parameters derived from microtremor arrays in the Western Plain of Taiwan. J Asian Earth Sci 128:27–41. https://doi.org/10.1016/j.jseaes.2016.07.012
Lacombe O, Mouthereau F, Angelier J, Deffontaines B (2001) Structural, geodetic and seismological evidence for tectonic escape in SW Taiwan. Tectonophysics 333:323–345. https://doi.org/10.1016/S0040-1951(00)00281-X
Liu Y, Li J, Fasullo J, Galloway DL (2020) Land subsidence contributions to relative sea level rise at tide gauge Galveston Pier 21, Texas. Sci Rep 10:1–11. https://doi.org/10.1038/s41598-020-74696-4
Lu C-Y, Hu J-C, Chan Y-C, Su Y-F, Chang C-H (2020) The relationship between surface displacement and groundwater level change and its hydrogeological implications in an alluvial fan: case study of the Choshui River, Taiwan. Remote Sens 12:3315. https://doi.org/10.3390/rs12203315
Martens HR (2016) using earth deformation caused by surface mass loading to constrain the elastic structure of the crust and mantle. Doctoral dissertation, California Institute of Technology, USA
Meckel T, ten Brink US, Williams SJ (2006) Current subsidence rates due to compaction of Holocene sediments in southern Louisiana. Geophys Res Lett 33. https://doi.org/10.1029/2006GL026300
Minderhoud P, Erkens G, Pham V, Bui VT, Erban L, Kooi H, Stouthamer E (2017) Impacts of 25 years of groundwater extraction on subsidence in the Mekong delta, Vietnam. Environ Res Lett 12:064006. https://doi.org/10.1088/1748-9326/aa7146
Parsons T (2006) Tectonic stressing in California modeled from GPS observations. J Geophys Res Solid Earth 111. https://doi.org/10.1029/2005JB003946
Poland JF (1984) Guidebook to studies of land subsidence due to groundwater withdrawal. United Nations Educational, Scientific and Cultural Organization (UNESCO), France
Shyu JBH, Sieh K, Chen YG, Liu CS (2005) Neotectonic architecture of Taiwan and its implications for future large earthquakes. J Geophys Res Solid Earth 110. https://doi.org/10.1029/2004JB003251
Taiwan WRA (2018) Monitoring and analyzing land subsidence of Taipei, Miaoli, Taichung, Chiayi, Pingtung and Ilan Area in 2018. Water Resources Agency, MOEA, Taiwan (in Chinese)
Teatini P, Strozzi T, Tosi L, Wegmüller U, Werner C, Carbognin L (2007) Assessing short-and long-time displacements in the Venice coastland by synthetic aperture radar interferometric point target analysis. J Geophys Res Earth Surf 112. https://doi.org/10.1029/2006JF000656
Teatini P, Tosi L, Strozzi T (2011) Quantitative evidence that compaction of Holocene sediments drives the present land subsidence of the Po Delta, Italy. J Geophys Res Solid Earth 116. https://doi.org/10.1029/2010JB008122
Törnqvist TE, Wallace DJ, Storms JE, Wallinga J, Van Dam RL, Blaauw M, Derksen MS, Klerks CJ, Meijneken C, Snijders EM (2008) Mississippi Delta

subsidence primarily caused by compaction of Holocene strata. Nat Geosci 1:173–176. https://doi.org/10.1038/ngeo129
Tran D-H, Wang S-J, Nguyen QC (2022) Uncertainty of heterogeneous hydrogeological models in groundwater flow and land subsidence simulations—a case study in Huwei Town, Taiwan. Eng Geol:106543. https://doi.org/10.1016/j.enggeo.2022.106543
Tran D-H, Wang S-J (2020) Land subsidence due to groundwater extraction and tectonic activity in Pingtung Plain, Taiwan. Proc Int Assoc Hydrol Sci 382:361–365. https://doi.org/10.5194/piahs-382-361-2020
Tran D-H (2020) Quantify Land Subsidence due to Groundwater Extraction and Tectonic Activity in Southwestern Taiwan. Master dissertation, National Central University
Tung H, Hu J-C (2012) Assessments of serious anthropogenic land subsidence in Yunlin County of central Taiwan from 1996 to 1999 by Persistent Scatterers InSAR. Tectonophysics 578:126–135. https://doi.org/10.1016/j.tecto.2012.08.009
Wang S-J, Lee C-H, Chen J-W, Hsu K-C (2015a) Combining gray system and poroelastic models to investigate subsidence problems in Tainan, Taiwan. Environ Earth Sci 73:7237–7253. https://doi.org/10.1007/s12665-014-3902-5
Wang S-J, Lee C-H, Hsu K-C (2015b) A technique for quantifying groundwater pumping and land subsidence using a nonlinear stochastic poroelastic model. Environ Earth Sci 73:8111–8124. https://doi.org/10.1007/s12665-014-3970-6
Wang M, Shen ZK (2020) Present-day crustal deformation of continental China derived from GPS and its tectonic implications. J Geophys Res Solid Earth 125:e2019JB018774. https://doi.org/10.1029/2019JB018774
Weber K, Stewart M (2004) A critical analysis of the cumulative rainfall departure concept. Ground Water 42:935. https://doi.org/10.1111/j.1745-6584.2004.t01-11-.x
Wu FT (1978) Recent tectonics of Taiwan. J Phys Earth 26:S265–S299. https://doi.org/10.4294/jpe1952.26.Supplement_S265
Yu S-B, Chen H-Y, Kuo L-C (1997) Velocity field of GPS stations in the Taiwan area. Tectonophysics 274:41–59. https://doi.org/10.1016/S0040-1951(96)00297-1
Zoccarato C, Minderhoud PS, Teatini P (2018) The role of sedimentation and natural compaction in a prograding delta: insights from the mega Mekong delta. Vietnam Sci Rep 8:1–12. https://doi.org/10.1038/s41598-018-29734-7

Publisher's Note